Available online at www.sciencedirect.com
SCIENCE DIRECT
Journal of Solid State Chemistry 179 (2006) 2426–2432
JOURNAL OF SOLID STATE CHEMISTRY
www.elsevier.com/locate/jssc

Synthesis, structure and magnetic properties of porous magnetic composite, based on MCM-41 molecular sieve with Fe_3O_4 nanoparticles

Sergey V. Kolotilov[a,*], Oleksiy Shvets[a], Olivier Cador[b], Natalia Kasian[a], Vyacheslav G. Pavlov[c], Lahcène Ouahab[b], Vladimir G. Ilyin[a], Vitaly V. Pavlishchuk[a]

[a]*L.V. Pisarzhevskii Institute of Physical Chemistry of the National Academy of Sciences of the Ukraine, Prospekt Nauki 31, Kiev 03028, Ukraine*
[b]*Equipe Organometallique et Matériaux Moléculaires, UMR 6226 CNRS-Université de Rennes 1, Campus de Beaulieu, 35042 Rennes cedex, France*
[c]*A.A. Blagonravov Institute of Mechanical Engineering, Malyy Kharitonovskiy lane 4, Moscow, 101830, Russia*

Received 9 March 2006; received in revised form 26 April 2006; accepted 27 April 2006
Available online 11 May 2006

Abstract

Porous magnetic composites were prepared by the synthesis of molecular sieve MCM-41 in the presence of Fe_3O_4 nanoparticles with average diameter of 15 nm. Nanoparticles were captured by porous silica matrix MCM-41, which resulted in their incorporation, as it was confirmed by TEM, SEM and X-ray diffraction. The materials possessed high surface area (392–666 $m^2 g^{-1}$), high pore volume (0.39–0.73 $cm^3 g^{-1}$) along with high magnetic response (M_S up to 28.4 emu g^{-1} at 300 K). Calcination of samples resulted in partial oxidation of Fe_3O_4 to α-Fe_2O_3. The influence of nanoparticles content on sorption and magnetic properties of the composites was shown. No hysteresis was found for the samples at 300 K; at 5 K, H_C was in the range 370–385 G for non-calcinated samples and 350–356 G for calcinated ones.

Keywords: Porous magnetic composites; Molecular sieves; MCM-41; Fe_3O_4 nanoparticles; Sorption properties; Magnetic properties

1. Introduction

Porous materials and molecular sieves attract much attention due to their remarkable characteristics, they possess high surface and high sorption capacity compared to non-porous objects, as well as the possibility to perform selective sorption of various substrates by regulation of pore diameter or easy chemical modification [1–3]. The most studied porous materials are those built from diamagnetic units, such as carbon, oxides of *p* elements, etc. [4,5]. Such porous materials are widely used in various fields, in particular, for sorption of different substrates from liquids with analytical, technical, environmental or biochemical purposes [6–9]. Creation of porous materials, which may be drawn into magnetic field, opens new fields of application of such species—they may be used for magnetic separation (extraction of adsorbed compounds from the solution) or transport of adsorbed compounds in magnetic fields [10–13], as well as for development of magnetochemical sensors [14,15]. Magnetic separation of the compound (porous carrier with adsorbed substrate) may significantly simplify analytical procedures, and in some cases it may provide the best way for separation of the compounds (for example, in the case of colloids, like blood). Some recent examples of such application include extraction of immunoglobulins by modified magnetic nanoparticles [16] and transport of anti-inflammatory agent ibuprofen by silica-coated magnetic microspheres [10].

For this purpose, the material should have significant ferro- or ferrimagnetic response, since "simple" paramagnetism is not sufficient for movement of the particles in magnetic fields, which are created by common permanent magnets. Two approaches may be proposed for the preparation of porous magnetic materials: (i) creation of magnetic particles in already prepared porous matrix and (ii) synthesis of porous component at the surface of magnetic nanoparticles.

*Corresponding author. Fax: +38 044 525 62 16.
E-mail address: svk001@mail.ru (S.V. Kolotilov).

0022-4596/$ - see front matter © 2006 Elsevier Inc. All rights reserved.
doi:10.1016/j.jssc.2006.04.039

The first approach may be illustrated by several examples. Nanoparticles of paramagnetic α-Fe_2O_3 in pores of SBA-15 were synthesized by thermolysis of $Fe(NO_3)_3$ inside the pores [17]. As expected, partial occupation of pores resulted in decrease of specific surface and volume of pores, giving rise to materials containing about 25% of Fe_2O_3. It should be noted that synthesis of nanoparticles in porous matrix should result in full or at least partial occupation of pores. Ordered material of MCM-41 type, containing 8.2 wt% of Fe, was prepared by introduction of $FeCl_3$ into reaction mixture [18]. Fe^{III} ions occupied tetrahedral positions in silica structure and no clustered Fe oxides were found, hence the material had the properties of simple paramagnet.

Regarding the second approach, superparamagnetic porous aluminosilicate with γ-Fe_2O_3 particles embedded in the walls was prepared by addition of Fe^{III} ethoxide powder to the reaction mixture, followed by calcination of the product [19]. Several methods for the synthesis of nanoparticles, covered by SiO_2, were reported. γ-Fe_2O_3 nanoparticles were covered by SiO_2 shell, forming composite species with an average diameter at 145 nm [20]. SiO_2 dissolution precipitation was used for covering α-Fe_2O_3 nanoparticles [21]. Mixed-oxide SiO_2–Fe_2O_3 nanocomposite was prepared by sol–gel method [22]. None of these materials exhibit magnetic response sufficient for magnetic separation from the solution combined with high sorption capacity.

Porous layer of MCM-41 structure was grown on Fe_3O_4 microparticles (3 μm in average), which allowed to achieve high magnetization (83 emu g^{-1} at room temperature) along with rather low surface (52.3 $m^2 g^{-1}$) [23]. Very recently, the magnetic porous microspheres were prepared by synthesis of porous silica on 12 nm Fe_3O_4 nanoparticles [10]. Such approach allowed to prepare the composite with high surface (721 $m^2 g^{-1}$) but comparatively low magnetization (about 2 emu g^{-1} at 300 K) [10]. Growth of mesoporous silica layer on Fe_2O_3 nanoparticles followed by reduction of this oxide to Fe_3O_4 also allowed to synthesize porous magnetic microspheres, containing 48-nm particles of Fe_3O_4 [13]. This sample possessed rather high surface (250 $m^2 g^{-1}$) along with high magnetization (9.8 emu g^{-1}) [13]; however, the synthesis was rather complicated.

Notably, magnetic materials may be synthesized by formation of porous structure from paramagnetic building blocks without "special" porous component, which may be illustrated by the synthesis of mesostructured iron oxyhydroxides [24,25] or paramagnetic porous coordination polymers [26]; however, magnetic responses of such compounds at room temperature are quite low for their use as magnetic sorbents.

The aim of this study was to develop a new method of porous magnetic material preparation by growth of porous silica matrix on Fe_3O_4 nanoparticle, and to find how magnetic properties of such materials depend on nanoparticles content and the conditions of sample treatment. The idea of such material preparation was to use magnetic nanoparticles, a priori much larger than pore diameter, in order to avoid pore filling and produce combination of ferrimagnetism with high surface area, capable of sorption of various substrates. For this purpose, we used 15-nm Fe_3O_4 particles (vide infra) and porous MCM-41 material with average pore size of about 3.3 nm. Since the distribution of magnetic nanoparticles by their size has no influence on desired properties of the material, we especially chose the simplest method for preparation of nanoparticles, realizing, however, that such distribution there will be broad. The materials, described in this paper, fill the interval between porous magnetic composites with high surface/low magnetization [10] and low surface/high magnetization [23], as well as allow us to see the influence of Fe_3O_4/Fe_2O_3 content on sorption and magnetic properties of ferrimagnetic porous composites.

2. Experimental

2.1. Starting materials and physical measurements

Commercially available reagents and solvents ("Ukrreakhim", "Aldrich") were used without additional purification. X-ray powder measurements were carried out on DRON-3M diffractometer (Cu*K*α radiation, filtered by nickel). Since the main expected field for application of MCM-41/Fe_3O_4 composite is extraction of various substrates from the solutions, surface characteristics were determined by sorption of methanol, which is more hydrophilic than nitrogen or argon; methanol sorption on MCM-41 gives surface parameters close to the ones determined by nitrogen sorption [27]. Adsorption isotherms were measured by weight method (methanol, 293 K) [28]. Fe_3O_4 nanoparticles were prepared using standard procedure by addition of the solution, containing equimolar quantities of $Fe_2(SO_4)_3 \cdot 9H_2O$ and $FeSO_4 \cdot 7H_2O$ [29], to hot solution of NaOH. Average size of the particles was estimated by Scherrer equation, which was proven to be correct for similar systems [30] and was independently confirmed by TEM. TEM studies were performed on Philips EM430 ST; instrument, SEM was performed on JEOL F-6301. Magnetic measurements were performed on Quantum design SQUID MPMSXL magnetometer with a maximum of 5 T and operating between 2 and 300 K.

2.2. Synthesis

The procedure for preparation of MCM-41 [31] was modified by introduction of nanoparticles in reaction mixture. Water solution of cetyltrimethylammonium chloride was adjusted to pH = 10.5 by ammonia, and then the calculated quantity (Table 1) of Fe_3O_4 colloid was added at vigorous stirring. The reaction mixture was charged with HS-40 silicasol, stirred for 0.5 h at room temperature,

followed by hydrothermal treatment at 100 °C during 3 h. Synthesized material was filtered off, washed with water and dried at room temperature to constant weight (samples **1–4**, Table 1), after which it was calcinated at 550 °C for 5 h (samples **1′–4′**, respectively). Fe_3O_4 nanoparticles from the same batch were used for the synthesis of materials, which allows to perform correct comparison of their physical properties.

3. Results and discussion

3.1. Synthesis and structure of the materials

Introduction of Fe_3O_4 sol in the reaction mixture, normally used for the synthesis of MCM-41, allowed to prepare materials with nanoparticles, attached to porous silica matrix (in the materials **1–4**, the pores were filled with cetyltrimethylammonium chloride). "Wet" method for nanoparticle preparation was chosen because it leads to the particles with hydrophilic surface, in contrast to the nano-oxides, synthesized by high-temperature decomposition of precursors [32]. It could be expected that the presence of hydroxo-groups on nanoparticle surface favored the covalent bonding to silica phase with possible formation of Si–O–Fe bonds and formation of composite rather than a mixture. Although it is difficult (or even impossible) to distinguish bonded nanoparticles and the mixture by TEM, the supposition about formation of Si–O–Fe bonds agrees with the data of magnetic measurements, vide infra. It is also worth to note that no separation between magnetic and non-magnetic phases was observed during sedimentation of sample suspensions in water in the field of permanent magnets.

Table 1
Composition and sorption characteristics of the materials

No.	Fe_3O_4 content (%)	BET surface area ($m^2 g^{-1}$)	BJH micropores volume ($cm^3 g^{-1}$)	BJH mesopores volume ($cm^3 g^{-1}$)
1	1.4	—	—	—
1′	1.8	666	0.1	0.73
2	4.2	—	—	—
2′	5.4	602	0.1	0.73
3	13.2	—	—	—
3′	18.0	526	0	0.51
4	24.0	—	—	—
4′	35.1	392	0	0.39

Among prepared materials, two groups may be distinguished. Materials **1**, **2** and **1′**, **2′** with low Fe_3O_4 content are almost white and reveal strong MCM-41 and weak Fe_3O_4 reflections in XRD patterns (Fig. 1). In contrast, materials **3** and **4** are black (**3′** and **4′** are brick-red) and show weak MCM-41 and strong Fe_3O_4 reflections. The reflections in 2θ range between 15° and 60° can be assigned to Fe_3O_4 for all samples. Naturally, their intensities increase with the Fe_3O_4 content; however, there is a sharp difference between the intensities of reflections at $2\theta = 35.7°$ for samples **2** and **3** (Fig. 1). In addition, iron X-ray fluorescence is weak for 1 and 2 and significant for 3 and 4. Since rather thin layer of the sample gives origin for both X-ray diffraction and X-ray fluorescence, it can be

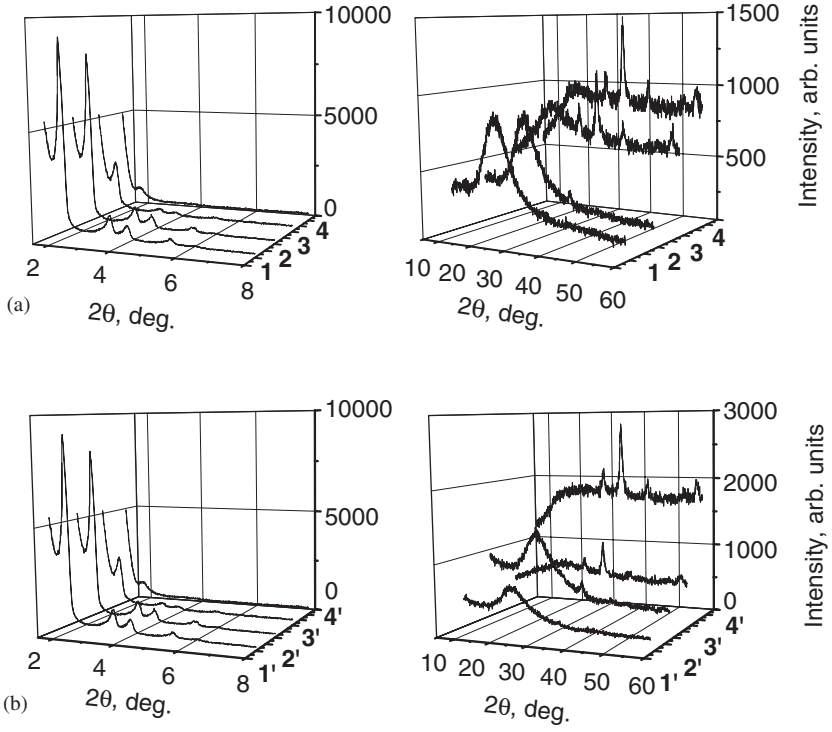

Fig. 1. X-ray diffraction patterns of samples before (a) and after (b) aerobic calcination.

supposed that nanoparticles are completely covered by SiO_2 in materials **1** and **2**, but some portions of Fe_3O_4 remain uncovered in **3** and **4** (or the layer of SiO_2 on the nanoparticles is very thin).

In all cases MCM-41 phase was formed, as it is evidenced by the reflections at $2\theta = 2.0^\circ$ (corresponding $d = 44$ Å in MCM-41, Fig. 1). The quality of the structure (intensities and half-widths of peaks at $2\theta = 2.0^\circ$, measured at the same conditions, as well as the presence of "satellites" in 2θ range between 3° and 6°) deteriorates with the growth in Fe_3O_4 content (which may evidence that Fe_3O_4 had influence on formation of silica phase), but for all samples studied the MCM-41 structure could be considered as highly ordered (which is also confirmed by TEM measurements, vide infra). Calcination of samples 1 and 2 resulted in improvement of MCM-41 ordering: after calcination, the peak at $2\theta = 2.0^\circ$ became two times more intensive. However, this was not observed for **3** and **4**, the intensity of this reflection did not change significantly after thermal treatment.

Change of sample's color from black to brick-red after calcination on air may be associated with oxidation of Fe_3O_4 to α-Fe_2O_3. However, positions and relative intensities of reflections in XRD patterns do not change: for example, the most intense peak in **4** and **4′** is found at $2\theta = 35.655(5)^\circ$ and $35.658(5)^\circ$, respectively. Along with this, average particle size, calculated for calcinated samples by Scherrer equation, is slightly smaller (14.5 nm) than for non-calcinated sample. It may be supposed that oxidation of surface layer of nanoparticles occurs. No new reflections, which may be assigned to Fe_2O_3, are detected, which can be explained by low content of this phase. However, the positions of the most intensive reflections of Fe_2O_3 and Fe_3O_4 are rather close, they should overlap at low content of one of these phases, so the presence of some portion of crystalline α-Fe_2O_3 cannot be excluded from XRD data.

TEM measurements of sample **3′** (Fig. 2a) showed that the material was not ideally homogeneous in length scale less than 100–200 nm. Nanoparticles of Fe_3O_4 were captured by MCM-41, preventing formation of its large crystals. Silica phase, surrounding the nanoparticles, is ordered, and clearly distinctive channels of MCM-41 over Fe_3O_4 can be observed. At the same time, there are some crystals of MCM-41 not attached to Fe_3O_4 nanoparticles. Diffuse edges of the nanoparticles on TEM image may be associated with formation of silica shells around them, similar to the results reported for silica-coated Fe_3O_4 microparticles [23]; this may be an additional proof of covalent bonding of Fe_3O_4 and silica component. According to TEM pictures, Fe_3O_4 nanoparticles have an average diameter of about 13 nm over 100 particles, which is close to the value calculated from XRD data. No aggregates of Fe_3O_4 could be detected, which is important for interpretation of magnetic data, vide infra. The diameter of 80% of particles is between 11 and 17 nm (Fig. 3).

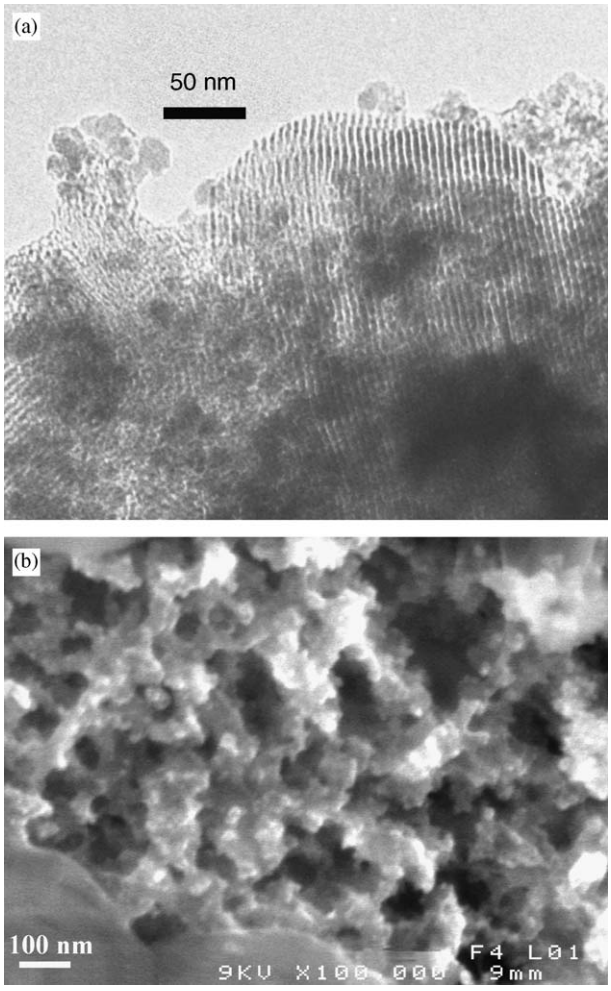

Fig. 2. TEM (a) and SEM (b) images of sample **3′**.

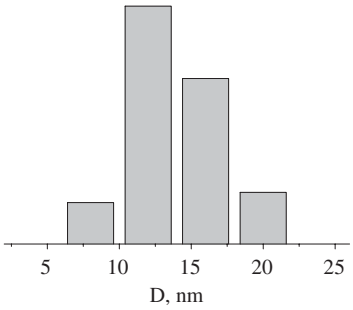

Fig. 3. Distribution of Fe_3O_4 nanoparticles by sizes according to TEM data.

Non-crystalline aggregates in the material, along with some portion of MCM-41 crystals, were found by SEM (Fig. 2b). Such aggregates probably represent the globules of Fe_3O_4 nanoparticles, covered by silica porous shells.

Thus, Fe_3O_4 nanoparticles are covered by crystalline MCM-41 or attached to such crystals in synthesized composite. Introduction of Fe_3O_4 nanoparticles into MCM-41 does not significantly destroy its porous structure. In all cases, nanoparticles do not fill the pores of MCM-41.

3.2. Adsorption characteristics of the materials

BET specific surface (S) of materials **1′–4′** lies in range between 392 and 666 $m^2 g^{-1}$ (Table 1), the volume of mesopores (V_{meso}) varies from 0.39 to 0.73 $cm^3 g^{-1}$ and average pore diameter in all cases is 3.5 nm, as determined by the Barrett–Joyner–Halenda method [33] (adsorption measurements of samples **1–4** are of no sense, because pores are filled with organic template). For nanoparticle-free MCM-41, synthesized in the same conditions, corresponding values are $S = 750\,m^2 g^{-1}$ and $V_{meso} = 0.77\,cm^3 g^{-1}$. Samples **1′** and **2′** are also characterized by rather significant volume of micropores (about 0.1 $cm^3 g^{-1}$ for each sample, estimated from t-plot).

Both S and V_{meso} of **1′–4′** non-linearly fall with the growth of Fe oxide content (Fe_3O_4 and Fe_2O_3, see above) (Fig. 4). The lines in Fig. 4 show the values, which are expected for a simple mixture of MCM-41 and corresponding quantity of Fe_3O_4, assuming that pure MCM-41 has surface area equal to 745 $m^2 g^{-1}$ and pore volume 0.77 $cm^3 g^{-1}$. To calculate these lines, we assumed that non-porous component (Fe_3O_4) reduces S and V of composite material due to simple dilution of porous component. Although it is rather rough approximation, there is clear tendency that the values of S and V are in all cases lower than expected ones, indicating that adsorption properties of some part of SiO_2 are worse than for highly ordered MCM-41. Two explanations can be proposed: (i) the layer of SiO_2, attached to the surface of nanoparticles, can be completely non-porous and acts as intermediate between Fe_3O_4 and ordered MCM-41 (ii) introduction of nanoparticles increases the disorder of MCM-41 structure or blocks a part of channels in MCM-41. Probably, both these factors take place. However, 2-fold increase of nanoparticle content (samples **3′** and **4′**) resulted in a decrease of V_{meso} from 0.51 to 0.39 $cm^3 g^{-1}$, indicating that the contribution of channels blocking is probably not significant.

Despite the reduction of S and V_{meso} compared to pure MCM-41 for **1′–4′**, these characteristics of the samples are still high for their application as sorbents.

3.3. Magnetic characteristics of samples

In order to study the influence of Fe_3O_4 content on magnetic properties of the materials, magnetic characterization of samples **1**, **3**, **3′**, **4** and **4′** was performed. Measurements of magnetization vs. temperature in ZFC mode for all samples showed broad maxima at T in the range 170–210 K (Fig. 1a), corresponding to the blocking temperature, T_B. ZFC and FC (10 Oe) curves merged at T_S about 300 K, indicating the temperature of transition of all magnetic particles to superparamagnetic state [34]. At all temperatures, magnetization values for calcinated samples are higher than for non-calcinated samples, as it is expected considering higher Fe content (result of the template elimination).

The field dependences of magnetization were studied at 5 and 300 K (Table 2). For non-calcinated materials (**3** and **4**), the increase of M_S is proportional to the increase of Fe content (Table 1). Calcination of **3** resulted in 1.36-fold growth of Fe content (due to elimination of organic template from pores), while M_S increased in 1.24 times (at 5 K). Similarly, for samples **4** and **4′**, Fe content grew in 1.46 times, but M_S grew just in 1.08 times. Such lag in M_S growth may be associated with partial oxidation of ferrimagnetic Fe_3O_4 into paramagnetic α-Fe_2O_3, as it was noted above. However, the value of M_S for calcinated samples is still high, confirming that dominating phase is Fe_3O_4 (except silica matrix).

Recalculation of saturation magnetization per 1 g of Fe_3O_4 gives values about 110 emu g^{-1} (300 K), which are slightly higher than it may be expected from literature data. For Fe_3O_4 particles, prepared by similar coprecipitation

Table 2
Magnetic characteristics of the materials

	1	3	3′	4	4′
M_S, emu g^{-1} (300 K)	0.31	13.5	17.8	23.9	28.4
M_S, emu g^{-1} (5 K)	0.44	18.0	22.4	32.3	34.9
H_C, G (300 K)	0	0	0	0	0
H_C, G (5 K)	375	385	350	369	356

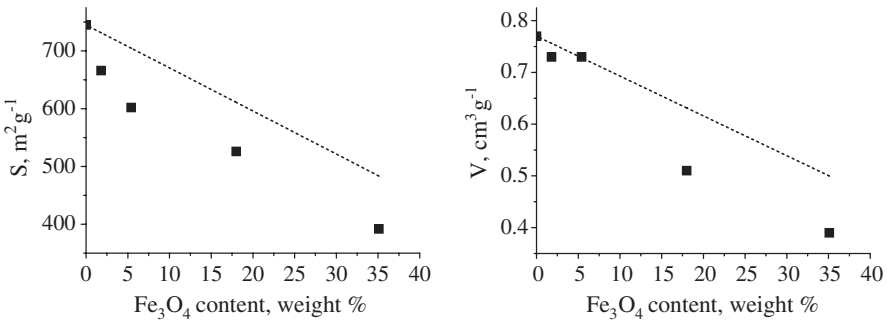

Fig. 4. Correlation of surface (S) and mesopore volume (V) with the content of Fe_3O_4 in the sample (lines represent the values, expected for the mixtures of MCM-41 and Fe_3O_4, see text).

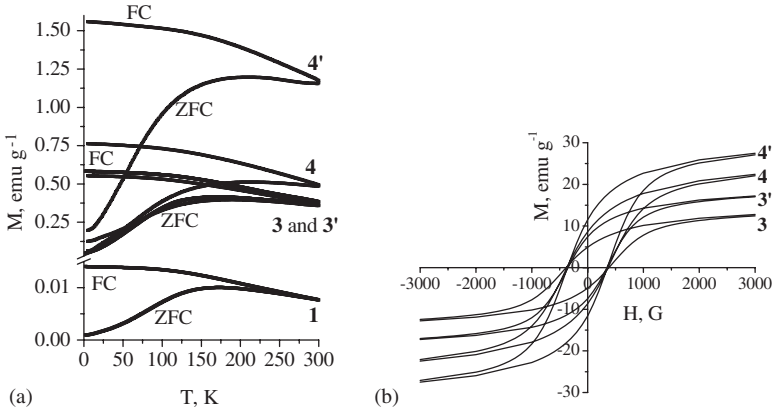

Fig. 5. ZFC and FC (10 Oe) dependencies of M vs. T of samples **1**, **3**–**4′** (a) and hysteresis loops of samples **3**–**4′** at 5 K (b).

from aqueous solutions of Fe^{II} and Fe^{III} salts with size distribution between 10 and 15 nm, containing 0.6 mol% of phosphatidylcholine, M_S was found to be 80 emu g^{-1} (300 K) [29]. Magnetite particles with average size of 28 nm, covered by oleic acid residues, were reported [35]. It was found that covering of these particles with SiO_2 resulted in an increase of M_S from 30 to 45 emu g^{-1}, which was attributed to reduction of weight fraction of diamagnetic compounds and to increased magnetic activity of the surface due to the formation of Fe–O–Si bonds [35]. Such increase of M_S correlates with the results of this study.

All studied samples showed no detectable hysteresis at 300 K, whereas at 5 K coercive field, H_C is found to be around 365 G (Fig. 5, Table 2). Coercivity is lower for calcinated samples, **3′** and **4′**, compared to non-calcinated species (Table 2). This is in line with the supposition about oxidation of surface of Fe_3O_4, since such oxidation should reduce the size of ferrimagnetic particles, which, in turn, should result in decrease of both M_S and H_C [36].

It was shown for Co nanoparticles confined in mesoporous silica matrix SBA-15 that uncouples magnetic particles were characterized by large increase of FC curves at temperature lowering [37]. In contrast, the coupling of magnetic nanoparticles resulted in a minor rise of FC curve and significant variation of H_C at the change of Co nanoparticle content [37]. Similar for all studied samples **2′**–**4′** change of FC curves vs. temperature, the absence of dependency of H_C on Fe content as well as linear growth of M_S for non-calcinated samples may be the evidence that there are no interactions between magnetic particles.

On the values of S and M_S, samples **3′** and **4′** take intermediate position between silica-coated 12 nm Fe_3O_4 particles ($S = 721\ m^2\ g^{-1}$, M_S about 2 emu g^{-1} [10]) and silica-coated 3 μm Fe_3O_4 ($S = 52.3\ m^2\ g^{-1}$, $M_S = 83$ emu g^{-1} [23]). Compared to silica-coated 48-nm Fe_3O_4 particles (12% Fe_3O_4, $S = 250\ m^2\ g^{-1}$, $M_S = 9.8$ emu g^{-1} [13]), both samples **3′** and **4′** have higher S and M_S values. While higher M_S in the latter case is consistent with higher content of Fe oxide in **3′** and **4′**, increased S may be associated with formation of MCM-41-like silica structure with average pore diameter of 3.5 nm in **3′** and **4′** instead of larger pore formation with average diameter equal to 6.03 nm in silica-coated 48-nm Fe_3O_4 particles [13].

4. Conclusions

In the result of this study, it was demonstrated that synthesis of mesoporous silica molecular sieves in the presence of magnetic nanoparticles could allow to prepare porous magnetic materials, possessing high surface, high pore volume along with high response to external magnetic field. It was shown that Fe_3O_4 nanoparticles are covered by silica component. The combination of sorption and magnetic properties may allow to consider synthesized species as promising sorbents for magnetic separation of various substrates from liquid media. Measurement of magnetic characteristics for the samples with varying Fe_3O_4 content showed that there were no interactions between the particles.

Acknowledgment

This work was partially supported by INTAS (Grant 03-51-4532).

References

[1] R. Szostak, Molecular Seives, Blackie Academic, London, 1998.
[2] K.J. Balkus, Prog. Inorg. Chem. 50 (2001) 217.
[3] T.D. Tilley, J. Mol. Catal. A: Chem. 182–183 (2002) 17.
[4] C. Yu, B. Tian, D. Zhao, Curr. Opin. Solid State Mater. Sci. 7 (2003) 191.
[5] M. O'Keeffe, O.M. Yaghi, Chem. Eur. J. 5 (1999) 2796.
[6] D. Wang, J. He, N. Rosenzweig, Z. Rosenzweig, Nano Lett. 4 (2004) 409.
[7] T.-J. Yoon, W. Lee, Y.-S. Oh, J.-K. Lee, New J. Chem. 27 (2003) 227.
[8] W. Zheng, F. Gao, H. Gu, J. Magn. Magn. Mater. 293 (2005) 199.
[9] A. del Campo, T. Sen, J.-P. Lellouche, I.J. Bruce, J. Magn. Magn. Mater. 293 (2005) 33.
[10] J. Kim, J.E. Lee, J. Lee, J.H. Yu, B.C. Kim, K. An, Y. Hwang, C.-H. Shin, J.-G. Park, J. Kim, T. Hyeon, J. Am. Chem. Soc. 128 (2006) 688.
[11] M. Šafaříková, I. Roy, M.N. Gupta, I. Šafařík, J. Biotechnol. 105 (2003) 255.
[12] M.-H. Liao, K.-Y. Wu, D.-H. Chen, Chem. Lett. 32 (2003) 488.

[13] Z. Zhang, L. Zhang, L. Chen, L. Chen, Q.-H. Wan, Biotechnol. Prog. 22 (2006) 514.
[14] K.G. Ong, M. Paulose, M.K. Jain, D. Gong, O.K. Varghese, C. Mungle, C.A. Grimes, Sensors 1 (2001) 138.
[15] L.S.-H. Ichia, E. Katz, J. Wasserman, I. Willner, Chem. Commun. (2002) 158.
[16] K. Holschuh, A. Schwämmle, J. Magn. Magn. Mater. 293 (2005) 345.
[17] F. Jiao, B. Yue, K. Zhu, D. Zhao, H. He, Chem. Lett. 32 (2003) 770.
[18] S. Samanta, S. Giri, P.U. Sastry, N.K. Mal, A. Manna, A. Bhaumik, Ind. Eng. Chem. Res. 42 (2003) 3012.
[19] C. Garcia, Y. Zhang, F. DiSalvo, U. Wiesner, Angew Chem. Int. Ed. 42 (2003) 1526.
[20] K. Kitajima, T. Fujita, N. Sogoshi, S. Nakabayashi, Chem. Lett. 33 (2004) 1106.
[21] S. Sato, R. Takahashi, T. Sodesawa, R. Tanaka, Bull. Chem. Soc. Japan 76 (2003) 217.
[22] B.J. Clapsaddle, A.E. Gash, J.H. Satcher Jr., R.L. Simpson, J. Non-Cryst. Solids 331 (2002) 190.
[23] P. Wu, J. Zhu, Z. Xu, Adv. Funct. Mater. 14 (2004) 345.
[24] G. Wirnsberger, K. Gatterer, H.P. Fritzer, W. Grogger, B. Pillep, P. Behrens, M.F. Hansen, C.B. Koch, Chem. Mater. 13 (2001) 1453.
[25] G. Wirnsberger, K. Gatterer, H.P. Fritzer, W. Grogger, B. Pillep, P. Behrens, M.F. Hansen, C.B. Koch, Chem. Mater. 13 (2001) 1467.
[26] J.L.C. Rowsell, O.M. Yaghi, Micropor. Mesopor. Mater. 73 (2004) 3.
[27] M.M.L. Ribeiro Carrott, A.J.E. Candeias, P.J.M. Carrott, P.I. Ravikovitch, A.V. Neimark, A.D. Sequeira, Micropor. Mesopor. Mater. 47 (2001) 323.
[28] N.V. Keltsev, Principles of Adsorption Methods, Khimiya, Moscow, 1984 (p. 1).
[29] J. Giri, S.G. Thakurta, J. Bellare, A.K. Nigam, D. Bahadur, J. Magn. Magn. Mater. 293 (2005) 62.
[30] Z. Li, H. Chen, H. Bao, M. Gao, Chem. Mater. 16 (2004) 1391.
[31] J.S. Beck, J.C. Vartuli, W.J. Roth, M.E. Leonowicz, C.T. Kresge, K.D. Schmitt, C. T-W. Chu, D.H. Olson, E.W. Sheppard, J.B. McCullen, J.B. Higgins, J.L. Schlenker, J. Am. Chem. Soc. 114 (1992) 10834.
[32] K.S. Gavrilenko, T.V. Mironyuk, V.G. Ilyin, S.N. Orlik, V.V. Pavlishchuk, Theor. Exp. Chem. 38 (2002) 110.
[33] E.P. Barrett, L.G. Joyner, P.P. Halenda, J. Am. Chem. Soc. 73 (1951) 373.
[34] J.A.L. Perez, M.A.L. Quintela, J. Mira, J. Rivas, S.W. Charles, J. Phys. Chem. B 101 (1997) 8045.
[35] K. Woo, J. Hong, J.-P. Ahn, J. Magn. Magn. Mater. 293 (2005) 177.
[36] C. Liu, A.J. Rondinone, Z.J. Zhang, Pure Appl. Chem. 72 (2000) 37.
[37] A.F. Gross, M.R. Diehl, K.C. Beverly, E.K. Richman, S.H. Tolbert, J. Phys. Chem. B 107 (2003) 5475.